ACS Applied Materials and Interfaces, Volume 7, Issue 24, June 2015, pp. 13512-13517
DOI: 10.1021/acsami.5b02790

Large energy-storage density and high temperature stability in high textured (111)-oriented $Pb_{0.8}Ba_{0.2}ZrO_3$ relaxor thin film with coexistence of antiferroelectric and ferroelectric

High textured (111)-oriented $Pb_{0.8}Ba_{0.2}ZrO_3$ (PBZ) relaxor thin film with coexistence of antiferroelectric and ferroelectric was prepared on $Pt/TiO_x/SiO_2/Si(100)$ substrate by using a sol-gel method. A large recoverable energy storage density of 40.18 J/cm^3 along with efficiency of 64.1% was achieved at room temperature. A high temperature stability of the energy storage density with variation of below 5% was obtained from room temperature to 250 ºC. The high energy storage performance was endowed by large dielectric breakdown strength, great relaxor dispersion, high texture orientation and the coexistence of the FE/AFE phases. The PBZ thin film is believed to be an attractive material for applications in energy storage systems in a wide temperature range.

Keywords: energy storage, relaxor, antiferroelectric, textured, sol-gel

1. Introduction

Recently, with the rapid development of microelectronic devices towards miniaturization, lightweight and integration, new dielectric capacitors with higher energy-storage density, fast charge/discharge and low cost, etc., are eagerly desired, due to the wide applications in power electronics and pulsed power systems, etc.[1-5] Antiferroelectrics (AFEs) have been predicted to might be a promising candidate for energy storage application as early as 1962.[2,6] However, little attention for a long time has been paid to them, because of the low energy storage density in their bulk

ceramics. For example, it was reported that the maximum energy storage density is only 2.75 J/cm^3.[7,8] It was recognized that the relatively low dielectric breakdown strength (normally less than 100 kV/cm) was one of the main reasons for the low energy-storage density.[9-11]

With the development of modern thin film technology such as sol-gel, pulsed laser deposition (PLD), and molecular beam epitaxy (MBE), etc., the higher dielectric breakdown strength can be achieved in thin or thick films.[4,5,12,13] Thus, the investigations on energy-storage properties of AFE films have reignited an attracted increasing attention. For instance, an improved energy-storage density of about 14 - 18 J/cm^3 was obtained in Pr, La, Sr, and Eu-doped $PbZrO_3$ thin film at room temperature.[14-17] Only recently, a huge energy density of 53 J/cm^3 and 56 J/cm^3 at about 3500 kV/cm was reported in relaxor antiferroelectric $(Pb_{0.92}La_{0.08})(Zr_{0.9}Ti_{0.05})O_3$ and $(Pb_{0.97}La_{0.02})(Zr_{0.55}Sn_{0.4}Ti_{0.05})O_3$ thick films, respectively.[1,5] In addition to the doping of elements and the optimization of compositions, other many efforts have been made to improve the value of the energy storage density in antiferroelectric films, such as, optimization of grain size, purification and crystallinity of phase, orientation of thin film, etc.[7,12-14,18-20] However, in practical applications, for a competent energy storage material, not only high value of energy storage density is required, but also high temperature stability is necessary. So far, to our knowledge, large energy storage density simultaneously with high temperature stability in antiferroelectric films is rarely reported.

In this study, a high textured, (111)-oriented $Pb_{0.8}Ba_{0.2}ZrO_3$ relaxor thin film with

coexistence of antiferroelectric and ferroelectric was fabricated by a sol-gel method. Large energy storage density (40.18 J/cm^3 at 2801 kV/cm) with high temperature stability (the variations of the energy density from room temperature to 250 ºC are below 5%) were achieved. Moreover, it is found that highly textured structure can greatly improve the energy storage performance.

2. Results and discussions

2.1. Structure

Fig.1 shows the XRD pattern of the PBZ thin film prepared by using the deposition way of layer-by-layer crystallization. The thin film exhibits a good crystallization quality and a pure perovskite phase with (111) preferential orientation. In addition to the rhombohedral ferroelectric phase, an orthorhombic antiferroelectric phase with superlattice reflections indices (130)/(112), (161)/(321) and (332) also coexisted in the PBZ thin film, which is consistent with the report by Pokharel.[21] Atomic force microscope (AFM) micrograph in the inset of Fig.1 reveals that the thin film has a low surface roughness, and the average Ra and Rq are 1.62 nm and 1.3 nm, respectively.[22]

Fig.2 shows the cross-sectional TEM image of the (111)-oriented PBZ thin film. The TEM cross-sectional image revealed that the microstructure of the PBZ thin film is uniform, homogeneous, and crack free, and with thickness of 320 nm. Nanocrystals with average grain size of 20 nm in a highly ordered columnar-like texture can be visible clearly in an enlarged image of the thin film, as shown in the inset (a) of Fig.2. In the inside of some nanocrystals, lamellar nanodomains with ~1 nm wide (the red dot circles) and ~2 nm wide (the blue solid circles) can be observed. The

corresponding selected area electron-diffraction (SAED) pattern which is labeled by using pseudo cubic rather than the orthorhombic or rhombohedral indicated that the columnar-like texture is (111)-oriented, as shown in the inset (b) of Fig.2.

2.2. Phase transition

In order to understand the structure change of the high textured (111)-oriented PBZ thin film, Raman scattering spectrum was measured from 100 cm^{-1} to 900 cm^{-1} at 5 K interval in the temperature range between 298 K and 463 K. Representative plots of them are shown in Fig. 3. Previous research work suggests that the appearance and change of the band at 277 cm^{-1} which is assigned to Zr-O-Zr bending mode can reflect the existence and change of antiferroelectric phase in $PbZrO_3$ thin film.[23] An additional active band at about 830 cm^{-1} was considered to be related to the appearance of the ferroelectric phase in 3% W-doping $PbZrO_3$ thin film.[23,24] For the highly textured (111)-oriented PBZ thin film, the Zr-O-Zr bending mode exhibits a slight shift due to internal stress in the film.[23] The inset (a) of Fig.3 shows the temperature dependence of the Zr-O-Zr bending mode. It can be seen that the scattering intensity of the Zr-O-Zr bending mode degraded gradually with the increase of temperature and disappeared at about 345 K, indicating that a phase transition of antiferroelectric to ferroelectric. Meanwhile, a wide band around 830 cm^{-1} was found to become more and more obvious with the increase of temperature, which further confirmed the existence of the phase transition of antiferroelectric to ferroelectric.[23] The phase transition of antiferroelectric to ferroelectric can also be observed on the maximum value of polarization versus temperature curve (P_{max}-T) by drawing on data from the P-E loops measured at 156 kV/cm, as shown in the inset (a) of Fig.3. The

more subtle phase transition process of antiferroelectric to ferroelectric can be detected by the temperature dependence of the dielectric permittivity and the dielectric loss of the highly textured (111)-oriented PBZ thin film, as shown by the red arrow in the inset (b) of Fig.3. The colored solid lines around the dielectric peak exhibited the best fitting result of the Lorentz-type relation, $\varepsilon_A/\varepsilon=1+(T-T_A)^2/2(\delta_A)^2$. The relevant detailed description on the equation could be found in previous research work.[25,26] A large parameter δ_A (97.73) for 10 kHz is obtained and is close to that (103.6) of the prototypical relaxor $Pb(Mg_{1/3}Nb_{2/3})O_3$ ceramics, indicating that a much higher degree of relaxor dispersion in the thin film. The extrapolated value at the left part of the dielectric peak is gradually far and below from its real value with the decrease in temperature from the phase transition of antiferroelectric to ferroelectric, which further indicates the coexistence of antiferroelectric and ferroelectric phases in PBZ thin film at room temperature.

2.3. Energy storage

The recoverable energy density (W_{energy}) of a dielectric-based compound could be estimated from the P-E loops, which is calculated with the following equation:

$$W_{energy} = \int_{Pr}^{P\max} EdP\ ,\quad 0 \le E \le E_{\max}\ ; \tag{1}$$

where E is the applied electric field that causes the variation in electric polarization P, P_r is the remnant polarization, and P_{max} is the maximum polarization under the applied field.[1-5] According to Eq. (1), materials simultaneously with smaller P_r, larger P_{max} and higher breakdown strength are more suitable for energy storage. They are realized in the highly textured (111)-oriented PBZ relaxor film through the

coexistence of FE and AFE phases, where the FE phase helps maintain a high P_{max}, the AFE phase keeps a low P_r, and the relaxation characteristic contributes to release the large phase transition stress.[27]

Fig. 4 shows the *P-E* loops of the highly textured $Pb_{0.8}Ba_{0.2}ZrO_3$ thin film at selected applied electric field. It can be seen that the *P-E* loop transformed gradually from a slim double hysteresis loop into a single hysteresis loop when the applied electric field increased from 156 kV/cm to 2801 kV/cm, indicating that a field-induced nanscale AFE to FE phase transition. The maximum polarization P_{max} and the remanant polarization P_r at 2801 kV/cm, is 19.76 μCcm^{-2} and 78.68 μCcm^{-2}, respectively. By integrating the discharging portion of the *P-E* loop according to Eq. (1), an energy density (W_{energy}) of 40.18 Jcm^{-3} (as painted by the cyan shaded area) at 2801 $kVcm^{-1}$ can be achieved on the highly textured (111)-oriented PBZ thin film.

For energy storage applications, good electric field endurance is another one of the crucial factors to consider for high energy-storage capacitors. The inset (a) in Fig. 4 depicts Weibull distribution of electric field strength for the highly textured PBZ thin film. The relevant detailed description on Weibull distribution could be found in previous research work.[28] According to the data given in the inset, a statistical breakdown strength values 2902 kV/cm can be obtained from the x intercept of the fitting lines. The high breakdown strength of samples was attributed to their denser microstructure.

In practical application, apart from higher recoverable energy density W_{energy} values, larger energy-storage efficiency (η) is also always desired, which is defined as the

ratio of the discharging (output) energy to the charging (input) energy,

$$\eta = W/(W + W_{Loss}); \quad (2)$$

where W_{loss} is the energy loss density, calculated by the numerical integration of closed area of the *P-E* hysteresis loops.[1-5] The inset (b) in Fig. 4 depeicts the electric field dependence of the energy density W_{energy}, the energy loss density W_{loss} and the energy-storage efficiency η. It can be seen that the W_{energy} increased gradually with the increase of the applied electric field and reached about 40.18 Jcm^{-3} at 2801 kV/cm, however, the W_{loss} increased first and then tended to be a constant about 22.5 Jcm^{-3} at 2801 kV/cm. Similar to the W_{energy}, the energy-storage efficiency η increased with the increase of the applied electric field and reached 64.1% at 2801 kV/cm. Assumed that a larger breakdown strength value could be achieved for the highly textured PBZ thin film, based on the above analysis results, it is easy to infer that a larger η could be achieved for the case of a constant W_{loss} under a larger electric field. The η can be further improved by an appropriate content of special elements doping, which can enhance the degree of relaxor dispersion and maintain the antiferroelectric property, such as rare earth element-La. Moreover, the η can also be enhanced by using oxide electrodes as contact electrodes such as $LaNiO_3$,[12] which can reduce the influence of the interfacial layer between film and contact electrode on the hysteresis loop of the film to obtain higher W_{energy} and lower W_{loss}.

In addition to the above mentioned, thermal stability of the energy-storage performance should also be considered as an important parameter in real capacitor applications. Fig.5 shows *P-E* loops of the highly textured $Pb_{0.8}Ba_{0.2}ZrO_3$ thin film in

a wide temperature range of 293-583 K, which is measured at 2726 kV/cm slightly lower than 2801 kV/cm to prevent from the high temperature thermal breakdown. The inset (a) of Fig.5 summarized the temperature dependence of the energy density W_{energy}, the energy loss density W_{loss} and the energy-storage efficiency η. Clearly, the W_{energy} increased slightly first from room temperature (39.17 Jcm^{-3}) up to 523 K (40.98 Jcm^{-3}) and then decreased sharply. The variations of the energy density W_{energy} from room temperature to 250 ºC are below 5% (as shown by the blue solid line), indicating good temperature stability of the energy-storage performance. The good temperature stability may be ascribed to the great relaxor dispersion of the highly textured PBZ thin film as shown in the inset (b) of Fig.3. Differently to the W_{energy}, the η decreased slowly first from room temperature (63.84%) up to 523 K (54.26%) and then dropped sharply. The variations of the η in the wide temperature range are about 15%. The two sharp decreases of the W_{energy} and the η above 523 K may be attributed to the reduction in polarization and the increase in leakage current (as shown by the round ends of the green *P-E* loop in Fig.5)

To get an insight into the effect of texture on the energy storage performance of the highly textured (111)-oriented PBZ thin film, a less textured PBZ thin film was prepared by adjusting the deposition process of thin film. Different from the deposition way of the layer-by-layer crystallization of the highly textured PBZ thin film, in the less textured PBZ thin film, each layer was dried at 350 °C for 3 min and then pyrolized at 550 °C for 5 min on hotplates, after the deposition of desired layers, the film was crystallized finally at 750 °C for 30 min in a tube furnace in air. As

shown by the inset (a) of Fig. 6, in addition to the diffraction of (111) (for convenience, the lattice indices are labeled as pseudo-cubic structure), very strong diffractions of (110) and (100) can also be detected in the XRD pattern, indicating the existence of a less textured film structure. The less textured film structure can also be confirmed by its cross-sectional TEM image and the corresponding SAED, as shown by the inset (b) of Fig. 6, where no obvious texture features can be detected.

Fig. 6 shows the *P*-*E* loops of the highly textured and less textured $Pb_{0.8}Ba_{0.2}ZrO_3$ thin film. A lower P_{max} (73.42 μCcm^{-2}) and a higher P_r (31.7 μCcm^{-2}) were obtained for the less textured PBZ thin film, as well as a bigger coercive field E_c (167 kV/cm). The W_{energy} and the η of the low textured PBZ thin film are 33.9 Jcm^{-3} and 37%, respectively. Compared to them in the less textured PBZ thin film, the W_{energy} (40.18 Jcm^{-3}) in the highly textured PBZ thin film was increased by 18.5% and the η (64.1%) was remarkably increased by 73.2%. These results indicate that highly textured structure can help improve the energy storage performance, especially in the energy efficiency η. Therefore, a larger W_{energy} and a higher η can be expected in a highly (111)-oriented single crystal PBZ thin film.

3. Conclusions

A large recoverable energy storage density of 40.18 J/cm^3 and simultaneously a high temperature stability (the variation of below 5% in the energy storage density from room temperature to 250 ºC) were achieved in the highly textured (111)-oriented $Pb_{0.8}Ba_{0.2}ZrO_3$ relaxor thin film with coexistence of antiferroelectric and ferroelectric. This is accomplished by the large dielectric breakdown strength, great relaxor

dispersion, high texture orientation and the coexistence of the FE/AFE phases. The excellent energy storage performance of the thin film may make it a promising material for applications in energy storage devices in a wide temperature range.

4. Experimental procedure

Fabrication of $Pb_{0.8}Ba_{0.2}ZrO_3$:

$Pb_{0.8}Ba_{0.2}ZrO_3$ (PBZ) thin film was grown by using a sol-gel method. $Pb(OAc)_2$ $3H_2O$ with 20% excesss Pb and $Ba(CH_3COO)_2$ were dissolved in glacial acetic and deionized water. Simultaneously, appropriate acetylacetone was added to a mixture of 2-methoxyethanol and $Zr(O^nPr)_4$. The Pb/Ba and Zr solutions were then mixed and stirred for 2 h at room temperature. The final concentration of the PBZ precursor solution is 0.3 M. After they aged for 24 h, the PBZ thin film was deposited on $Pt(111)/TiO_x/SiO_2/Si(100)$ substrate through a multiple-step spin-coating technique. Each layer of PBZ film was spin-coated at 4000 rpm for 30 s. To eliminate the formation of cracks, every wet film was first dried at 350 ºC for 3 min and subsequently pyrolyzed at 550 ºC for 3 min on hotplates, and finally crystallized at 800 ºC for 3 min in a tube furnace in air. Layer-by-layer, the spin-coating and heat-treatment were repeated several times to obtain the desired thickness. The final thickness of the PBZ thin film was about 320 nm determined by the crossing-section micrographs.

Characterization:

The crystallinity of the PBZ thin film was analyzed by X-ray diffraction (XRD, Rigaku 9 KW Smartlab, Japan). The cross-sectional morphology of the film was

examined by scanning electron microscope (SEM, FEI Sirion 200). The microstructure of the film was studied by transmission electron microscopy (TEM; JEOL JEM-2100F). The out-of-plane feature of the film was investigated by scanning probe microscope (SPM; Bruker Multimode 8).The Raman scattering spectra was acquired by Raman spectrometer (Horiba HR800) with excitation source of 488 nm laser. For the measurements of electrical properties, Au/Cr layers of 150 μm in diameter were evaporated on the surface through a patterned photoresist mask to form sandwich electrode structure. Dielectric permittivity measurement were carried out using an impedance analyzer (Wayne-Kerr Electronics, West Sussex, UK) with a perturbation voltage V_{ac} = 100 mV. Polarization-electric field hysteresis loops (*P*-*E*) and current-voltage curves (*I*-*V*) were obtained by means of a ferroelectric tester (Precision Premier Ⅱ, Radiant Technologies Inc.) at 10 kHz. The energy storage performance was calculated according to the *P*-*E* results.

Supporting Information

Supporting Information is available from the Wiley Online Library or from the author.

Acknowledgements

This work was supported by the Hong Kong Polytechnic University (Project Nos.: A-PL54, G-UC69 and 1-ZVCG), the National Natural Science Foundation of China (51402196, 51272161, 51172187), the China Postdoctoral Science Foundation (006858), and the Shenzhen Science and Technology Research Foundation (CXB201005240010A), 111 Program (B08040) of MOE,.

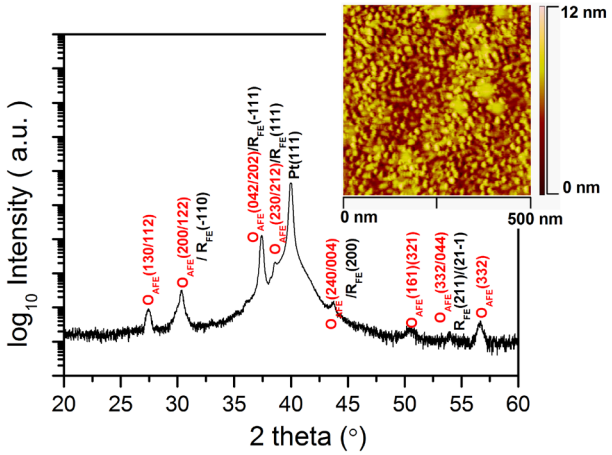

Figure 1. XRD pattern of the high textured (111)-oriented $Pb_{0.8}Ba_{0.2}ZrO_3$ thin film. Inset: AFM micrograph.

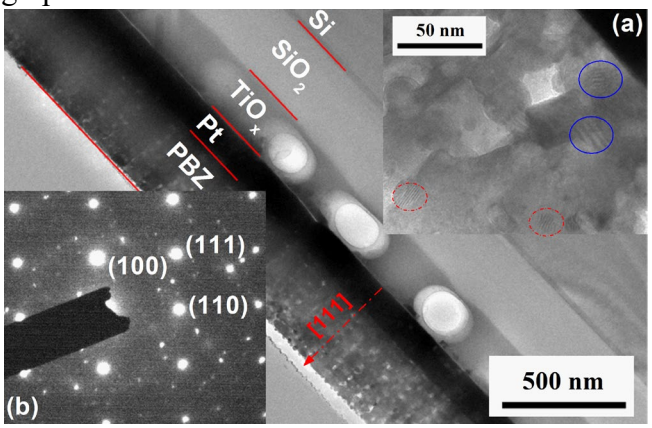

Figure 2. Cross-sectional TEM image of the high textured (111)-oriented $Pb_{0.8}Ba_{0.2}ZrO_3$ thin film. Inset: (a) an enlarged image of thin film (b) the corresponding SAED.

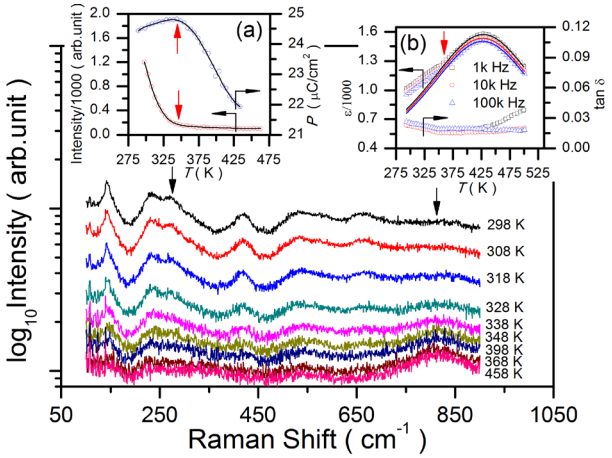

Figure 3. Raman scattering spectra of the high textured (111)-oriented $Pb_{0.8}Ba_{0.2}ZrO_3$ thin film. Inset: (a) Temperature dependences of the Zr-O-Zr bending mode and the P_{max} measured at 156 kV/cm and (b) $\varepsilon(T)$ and tan $\delta(T)$.

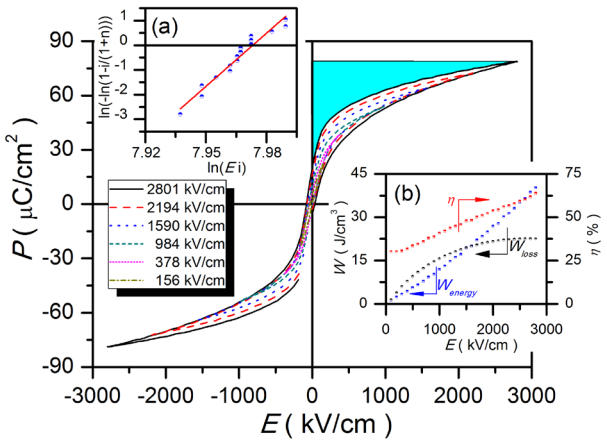

Figure 4. *P-E* loops of the high textured (111)-oriented $Pb_{0.8}Ba_{0.2}ZrO_3$ thin film at selected applied electric fields. The shaded area represents 40.18 Jm^{-3} being stored. Inset: W_{energy}, W_{loss} and η & E.

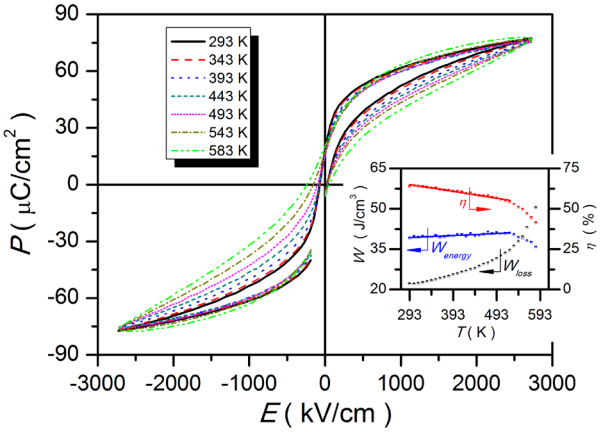

Figure 5. *P-E* loops of $Pb_{0.8}Ba_{0.2}ZrO_3$ thin film at selected temperatures. Inset: W_{energy}, W_{loss} and η vs. T.

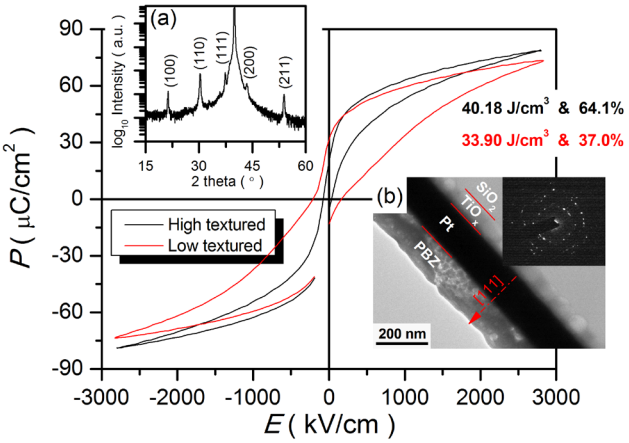

Figure 6. *P-E* loops of high textured and low textured $Pb_{0.8}Ba_{0.2}ZrO_3$ thin film. Inset: (a) XRD pattern and (b) cross-sectional TEM image and the corresponding SAED of low textured $Pb_{0.8}Ba_{0.2}ZrO_3$ thin film.

1. Zhao, Y., Hao, X. & Zhang, Q. Energy-Storage Properties and Electrocaloric Effect of Pb(1-3x/2)LaxZr0.85Ti0.15O3 Antiferroelectric Thick Films. *ACS Appl. Mat. Interfaces* **6**, 11633-11639 (2014).
2. Hao, X., Zhai, J., Kong, L. B. & Xu, Z. A comprehensive review on the progress of lead zirconate-based antiferroelectric materials. *Prog. Mater Sci.* **63**, 1-57 (2014).
3. Chu, B. J. *et al.* A dielectric polymer with high electric energy density and fast discharge speed. *Science* **313**, 334-336 (2006).
4. Correia, T. M. *et al.* A Lead-Free and High-Energy Density Ceramic for Energy Storage Applications. *J. Am. Ceram. Soc.* **96**, 2699-2702 (2013).
5. Ma, B., Kwon, D.-K., Narayanan, M. & Balachandran, U. Dielectric properties and energy storage capability of antiferroelectric $Pb_{0.92}La_{0.08}Zr_{0.95}Ti_{0.05}O_3$ film-on-foil capacitors. *J. Mater. Res.* **24**, 2993-2996 (2011).
6. Burn, I. & Smyth, D. M. Energy storage in ceramic dielectrics. *J Mater Sci* **7**, 339-343 (1972).
7. Zhang, L. *et al.* Y doping and grain size co-effects on the electrical energy storage performance of (Pb0.87Ba0.1La0.02) (Zr0.65Sn0.3Ti0.05)O3 anti-ferroelectric ceramics. *Ceram. Int.* **40**, 5455-5460 (2014).
8. Tuttle, B. A. & Payne, D. A. THE EFFECTS OF MICROSTRUCTURE ON THE ELECTROCALORIC PROPERTIES OF PB(ZR,SN,TI)O3 CERAMICS. *Ferroelectrics* **37**, 603-606 (1981).
9. Li, X., Xi, Z., Long, W. & Fang, P. Synthesis of antiferroelectric $(Bi_{0.534}Na_{0.5})_{0.94}Ba_{0.06}TiO_3$ ceramics with high phase transition temperature and broad temperature range by a solid-state reaction method. *Chin. Sci. Bull.* **58**, 2893-2897 (2013).
10. Gao, F. *et al.* Energy-Storage Properties of $0.89Bi_{0.5}Na_{0.5}TiO_3$-$0.06BaTiO_3$-$0.05K_{0.5}Na_{0.5}NbO_3$ Lead-Free Anti-ferroelectric Ceramics. *J. Am. Ceram. Soc.* **94**, 4382-4386 (2011).
11. Mischenko, A. S., Zhang, Q., Scott, J. F., Whatmore, R. W. & Mathur, N. D. Giant electrocaloric effect in thin-film PbZr(0.95)Ti(0.05)O3. *Science* **311**, 1270-1271 (2006).
12. Ge, J., Dong, X., Chen, Y., Cao, F. & Wang, G. Enhanced polarization switching and energy storage properties of Pb0.97La0.02(Zr0.95Ti0.05)O3 antiferroelectric thin films with LaNiO3 oxide top electrodes. *Appl. Phys. Lett.* **102**, 142905 (2013).
13. Hao, X., Zhou, J. & An, S. Effects of PbO Content on the Dielectric Properties and Energy Storage Performance of $(Pb_{0.97}La_{0.02})(Zr_{0.97}Ti_{0.03})O_3$ Antiferroelectric Thin Films. *J. Am. Ceram. Soc.* **94**, 1647-1650 (2011).
14. Sa, T., Qin, N., Yang, G. & Bao, D. Structure and improved electrical properties of Pr-doped PbZrO3 antiferroelectric thin films with (111) preferential orientation. *Mater. Chem. Phys.* **139**, 511-514 (2013).
15. Parui, J. & Krupanidhi, S. B. Enhancement of charge and energy storage in

sol-gel derived pure and La-modified PbZrO3 thin films. *Appl. Phys. Lett.* **92** (2008).

16. Hao, X., Zhai, J. & Yao, X. Improved Energy Storage Performance and Fatigue Endurance of Sr-Doped PbZrO3 Antiferroelectric Thin Films. *J. Am. Ceram. Soc.* **92**, 1133-1135 (2009).
17. Ye, M. *et al.* Effect of Eu Doping on the Electrical Properties and Energy Storage Performance of $PbZrO_3$ Antiferroelectric Thin Films. *J. Am. Ceram. Soc.* **94**, 3234-3236 (2011).
18. Parui, J. & Krupanidhi, S. B. Enhancement of charge and energy storage in sol-gel derived pure and La-modified PbZrO[sub 3] thin films. *Appl. Phys. Lett.* **92**, 192901 (2008).
19. Ge, J. *et al.* Enhancement of energy storage in epitaxial PbZrO3 antiferroelectric films using strain engineering. *Appl. Phys. Lett.* **105** (2014).
20. Ge, J. *et al.* Effect of residual stress on energy storage property in PbZrO3 antiferroelectric thin films with different orientations. *Appl. Phys. Lett.* **103** (2013).
21. Pokharel, B. P. & Pandey, D. High temperature x-ray diffraction studies on antiferroelectric and ferroelectric phase transitions in (Pb[sub 1−x]Ba[sub x])ZrO[sub 3] (x=0.05,0.10). *J. Appl. Phys.* **90**, 2985 (2001).
22. Pandey, S. K. *et al.* Structural, ferroelectric and optical properties of PZT thin films. *Physica B* **369**, 135-142 (2005).
23. Sa, T., Qin, N., Yang, G. & Bao, D. W-doping induced antiferroelectric to ferroelectric phase transition in PbZrO3 thin films prepared by chemical solution deposition. *Appl. Phys. Lett.* **102** (2013).
24. Pasto, A. E. & Condrate, R. A. Raman Spectrum of PbZrO3. *J. Am. Ceram. Soc.* **56**, 436-438 (1973).
25. Ke, S., Fan, H., Huang, H. & Chan, H. L. W. Lorentz-type relationship of the temperature dependent dielectric permittivity in ferroelectrics with diffuse phase transition. *Appl. Phys. Lett.* **93** (2008).
26. Peng, B., Fan, H., Zhang, Q. & Tan, X. The Contribution of the “Extrinsic” Polarizations to the Dielectric Tunability of Pb(Mg1/3Nb2/3)1−xTixO3 Relaxor Ferroelectrics. *J. Am. Ceram. Soc.* **95**, 1651-1655 (2012).
27. Zhang, Q. M., Bharti, V. & Zhao, X. Giant Electrostriction and Relaxor Ferroelectric Behavior in Electron-Irradiated Poly(vinylidene fluoride-trifluoroethylene) Copolymer. *Science* **280**, 2101-2104 (1998).
28. Zhao, Y., Hao, X. & Li, M. Dielectric properties and energy-storage performance of (Na-0.Bi-5(0).(5)) TiO3 thick films. *J. Alloys Compd.* **601**, 112-115 (2014).

2015-05-21

Large Energy Storage Density and High Thermal Stability in a Highly Textured (111)-Oriented Pb0.8Ba0.2ZrO3 Relaxor Thin Film with the Coexistence of Antiferroelectric and Ferroelectric Phases

Peng, Biaolin

American Chemical Society

Peng B, Zhang Q, Li X, et al., (2015) Large Energy Storage Density and High Thermal Stability in a Highly Textured (111)-Oriented Pb0.8Ba0.2ZrO3 Relaxor Thin Film with the Coexistence of Antiferroelectric and Ferroelectric Phases, ACS Applied Materials and Interfaces, Volume 7, Issue 24, June 2015, pp.13512-13517

http://dx.doi.org/10.1021/acsami.5b02790